IEEE Robotics and Automation Letters (RAL) paper presented at
2024 IEEE/RSJ International Conference on Intelligent Robots and Systems (IROS)
October 14-18, 2024. Abu Dhabi, UAE

A Wearable Finger Tremor-Suppression Orthosis Using the PVC Gel Linear Actuator

Chen Liu *Student Member, IEEE*, Ketao Zhang *Member, IEEE*

***Abstract*—Tremor is a prevalent neurological disorder that affects individuals of almost all ages and can significantly impede their quality of life and occupational functioning. Wearable medical devices for suppressing tremors, typically low-frequency vibrations ranging between 3 and 12 Hz, are gaining popularity since active vibration absorbers integrated into such devices have demonstrated immediate efficacy and noninvasive nature. However, there are challenges in miniaturizing active absorbers for wearable applications with traditional actuators. To address this problem, here we present a light wearable active finger tremor-suppressing orthosis (AFTO) that consists of a stacked polyvinyl chloride (PVC) gel actuator-based absorber, an inertial measurement unit (IMU), and a force sensor. The integrated sensors allow the device to detect tremors and trigger the absorber to suppress vibrations, regardless of whether the fingertip is vibrating in the air or applying tremor force while in contact with an object. A 3D-printed compliant Sarrus-mechanism exoskeleton was used to house the PVC gel stacked actuator, thus minimizing the linear actuator's swaying while maximizing the effective actuation area. This innovative wearable finger tremor absorption system has the potential for various applications in daily life and occupational contexts, such as stabilizing the finger during grasping, typing, operating surgical instruments, drawing, and other tasks.**

***Index Terms*—Tremor, orthosis, Sarrus mechanism, soft actuator, sensor.**

I. Introduction

TREMORS are present at all ages and severely impact people's quality of life [1], [2]. Due to complex causes of tremors, they are difficult to cure [3]. Although medication and surgery are being explored as treatment options, many patients are turning to external aids that suppress vibration as a less invasive and relatively safe alternative [4]–[6]. Stabilization devices capable of suppressing tremors are essential in specific daily life and work tasks, such as operating a scalpel, using forceps, or drawing.

According to the principle of tremor suppression, absorption devices are divided into three categories: passive, semi-active, and active [7]. Passive devices employ fixed damping, which can effectively eliminate most tremors, but the wearing comfort is challenging to adjust [8]–[10]. Semi-active devices using variable damping and stiffness methods can suppress tremors without affecting normal movement and are more comfortable to wear. However, residual vibration, especially at low frequencies, is still difficult to eliminate [11], [12]. Active absorbing devices are suitable for low-frequency vibration damping. However, there are rare explorations on vibration-absorbing devices for fingers as far as research is concerned, especially the closed-loop controlled active absorbing system [13], [14]. In addition, vibration absorbers driven by electric motors generally are large, heavy, and uncomfortable to carry [15], [16].

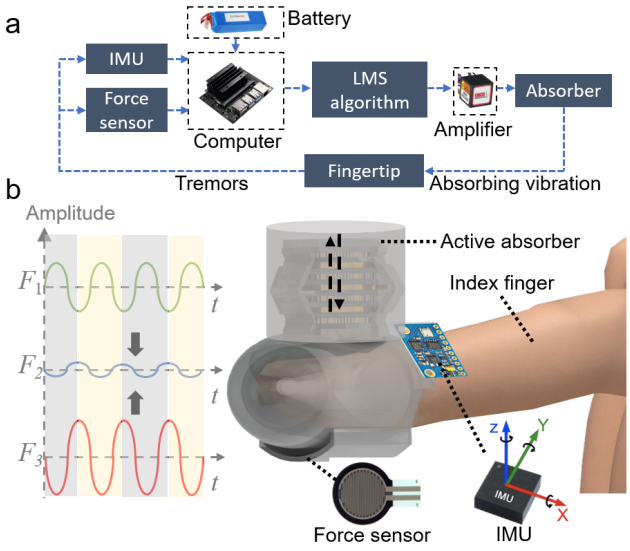

Fig. 1. The working principle and components of the AFTO. (a) The working process of suppressing the fingertip's tremors. (b) 3D models of AFTO components: a finger, vibration signals, the active actuator, the Surrus-mechanism exoskeleton, an IMU, and a force sensor.

Electric soft actuators have developed very rapidly in recent years [17]–[19]. Compared with rigid-body actuators, these new actuators have the advantages of small size, less heat generation, and soft texture [17]. In addition, they have a fast response (<0.1 s), making them ideal for making active vibration absorbers [20], [21]. However, the operating voltage of those actuators is generally high. For instance, the applied voltage to drive the dielectric elastomer actuator (DEA) [22], [23], HASEL artificial muscle [24], [25], and other smart actuators [26] are around and even over 10 kV. Among electric soft actuators, the polyvinyl chloride (PVC) gel actuator is notable for its ability to achieve output forces and response speeds of similar size while using lower voltages (a few hundred volts) than other electric soft actuators [27]. Re-

Manuscript received: November 9, 2023; Revised: January 14, 2024; Accepted: February 1, 2024.

This paper was recommended for publication by Editor Cecilia Laschi upon evaluation of the Associate Editor and Reviewers' comments. This work is partially funded by the Royal Society International Exchanges Cost Share award EC\NSFC\211324, Queen Mary Impact Fund, and China Scholarship Council (CSC) PhD Scholarship. *(Corresponding author: Ketao Zhang.)*

Chen Liu and Ketao Zhang are with the Centre for Advanced Robotics at Queen Mary University of London, UK chen.liu@qmul.ac.uk, ketao.zhang@qmul.ac.uk

Digital Object Identifier (DOI): see top of this page.

searchers have developed various wearable robotic devices by stacking PVC gel actuators and have achieved good actuation effects [28], [29]. However, due to the PVC gel actuator itself being composed of multiple materials (PVC gel, metal mesh, metal sheets), there has been no efficient housing method to guarantee linear actuation without getting loose. Previously, the stacked PVC gel actuator was wrapped with string or tape and this housing method was unreliable because the linearity of the actuation could not be guaranteed, and each wrapping would bring a different preload, resulting in unpredictable actuation performance [30]. Another interesting way is to use a straight stick through the center of the actuator, which could ensure that the actuator was stable and did not come loose while ensuring linear actuation [31], [32]. However, the housing method sacrifices some actuation performance because of the reduced adsorption area and produces friction between the stick and actuators, which degrades the actuation effect [30]. To deal with those issues, we bring forward a novel approach by integrating the stacked PVC gel actuator with a Sarrus mechanism [33], which houses the actuator and guarantees the maximum actuation area. Based on that, we introduce a new wearable active finger tremor-suppressing orthosis (AFTO) consisting of a stacked PVC gel actuator, a force sensor, and an inertial measurement unit (IMU).

The main contributions of the paper are:

1) A closed-loop controlled active finger tremor absorbing device, using the stacked PVC gel actuator, a force sensor, and an IMU is proposed for the first time.
2) The 3D-printed Sarrus-mechanism exoskeleton resolves the loose arrangement of the stacked PVC gel actuator without sacrificing the actuation layers area and minimizes undesired swaying of the linear actuator.
3) The integration of an IMU and a force sensor allows for tremor detection, regardless of whether the fingertip is vibrating free of contact or exerting tremor-inducing pressure in contact with an object.

The ensuing sections provide further details on the concept of the AFTO in the section II, the absorber, the Sarrus-mechanism exoskeleton, and the control scheme in the section III, tremor suppression simulations, tests, and the comparison with other finger tremor absorbers within the section IV.

II. The Concept of the AFTO

Since the main tremor direction of the fingertip is along the direction perpendicular to the nail surface [5], [15], we propose to use a wearable active absorber installed on the back of the fingertip to avoid affecting the finger's grasp of objects, as shown in Fig. 1(b), to suppress tremors. To monitor the tremor vibration and differentiate it from the normal finger action, an IMU (Digilent Pmod NAV: 9-axis IMU Plus, Digilent, USA) is integrated with the orthosis, as shown in Fig. 1(b), to detect vibration frequencies of the finger when the finger is free of contact with objects at a fixed position. Further, a force sensor (FSR07BE, OHMITE, USA) affixed under the fingertip (Fig. 1(b)) enables the detection of tremors when the finger is touching or operating an object, e.g. clicking the mouse (Fig. 2(b)), even though there is no obvious displacement of the finger.

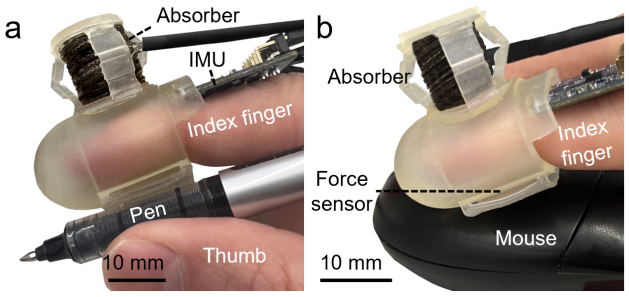

Fig. 2. Wearing effect displays of the AFTO in various applications: (a) when the index finger and the thumb are gripping a pen to write, the IMU on the back of the index finger helps to detect tremors by identifying frequencies of shaking, then the absorber on the top of the index finger is actuated to suppress tremors; (b) when the index finger clicking a mouse, the force sensor under the fingertip helps to detect tremors by identifying the frequency of the contacting pressing, then the absorber is triggered to suppress tremors to prevent unwanted clicking.

Fig. 1(a) illustrates the AFTO's operational procedure. The sensors detect the force (by the force sensor) and movement (by the IMU) of the finger and decide whether it is a tremor via a Least Mean Square (LMS) algorithm [34], which runs in the computer (Jetson Nano, NVIDIA Corporation, USA). If the detected frequency is less than 3 Hz, it is classified as a normal intended finger action. In contrast, it is considered a tremor when the frequency is over or equal to 3 Hz. Then the active actuator is triggered by the high voltage generated by the amplifier (Q10-5 DC, XP Power, UK) to produce vibrations with the same frequency but opposite phase as the tremor to suppress it.

Tremors are generally vibrations [2] and cause fingers to vibrate in a pattern of a single degree of freedom movement along the plane perpendicular to the nail surface. The frequency of such vibrations is usually under 12 Hz [1]. According to the classic theory for vibrations [35], the tremor force can be described as a simple harmonic force given by

$$F_1 = A_1 \ sin\omega t \tag{1}$$

where F_1 is the tremor force, A_1 is the amplitude, ω is the tremor's angular velocity, and t is the time.

The vibration force produced by the absorber has an opposite phase and is given by

$$F_2 = A_2 \ sin(\omega t + \pi) \tag{2}$$

F_2 is the vibration force produced by the absorber, and A_2 is the amplitude. The phase of the absorber is π out of phase with that of the tremor.

When the two vibration forces F_1 and F_2 happen in the same position, the resultant vibration force is yielded as F_3.

$$F_3 = F_1 + F_2 = A_3 \ sin\omega t = (A_1 - A_2) sin\omega t \tag{3}$$

where A_3 is the new amplitude, which is the difference between A_1 and A_2.

III. Design and System of the AFTO

In this work, we design a stacked PVC gel actuator capable of generating low-frequency vibration to drive the active absorber. The IMU and the force sensor are employed to detect the tremor frequency. The exoskeleton for housing the stacked actuator and the finger's ring is fully 3D printed with a flexible material (Elastic 50A Resin, Formlabs, USA), allowing it to adapt to various-sized fingers.

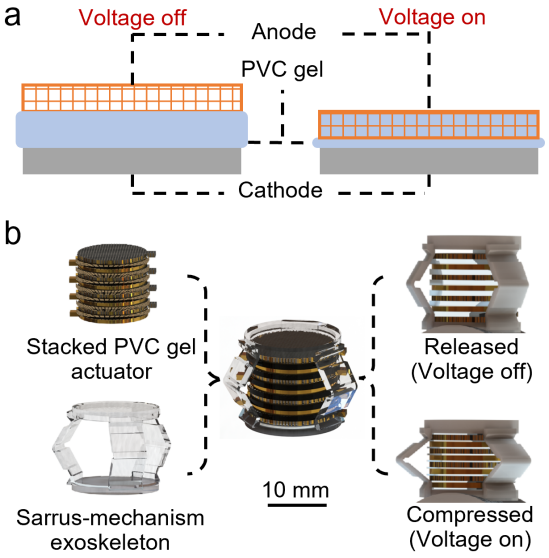

Fig. 3. (a) Schematic shows the actuation principle of one PVC gel actuator unit: applying voltages to the mesh, which absorbs the PVC gel and decreases the structure's height. (b) The new housing method for the stacked actuator: affix the stacked actuator into the Sarrus-mechanism exoskeleton.

A. Actuator for the Active Absorber

The active absorber is a PVC gel-stacked actuator with multiple units. Each unit consists of three layers stacked in the sequence of the anode metal mesh-PVC gel layer-cathode (one anode layer, one gel layer, and one cathode layer) (Fig. 3(a)). It can absorb the PVC gel into the mesh, and the thickness of the actuator will decrease when applying the voltage to the anode [36], [37]. Based on the requirement that the dimensional area of the entire absorber should not exceed the width of the finger (average in 15 mm [38]) (two adjacent fingers will not affect each other when they are held together), we designed the actuator with a diameter of 14 mm. According to relevant studies [39]–[41], the tremor force of the index fingertip is generally around 1 mN. With a tremor force of 1 mN, the number of units can be determined.

Assuming the vibration's cycle time as T, then the time t to experience the maximum stroke Δh of the stacked actuator is half of T, that is

$$t = \frac{T}{2} = \frac{1}{2f} \tag{4}$$

Given the symmetrical structure, the stacked actuator's geometric center is also the mass center. Hence, a maximum stroke of the center of mass Δh_c is half of Δh, meaning

$$\Delta h = 2\,\Delta h_c \tag{5}$$

If the initial velocity of the absorber is zero, Δh_c can also be expressed as

$$\Delta h_c = \frac{1}{2} a\, t^2 \tag{6}$$

where a is the acceleration of the actuation. Hence, the vibration force F produced by the stacked actuator can be described as

$$F = m\,a = 4\,m\,\Delta h\,f^2 \tag{7}$$

where the absorber's mass is m and the frequency is f.

Under the premise that the maximum displacement generated by each PVC gel actuator unit is determined, the more units, the greater the displacement generated per actuation at the same voltage. As a result, it gets greater acceleration and vibration force. To get the height of the structure determined by the number of PVC gel units, a system for testing the vibration force of the stacked actuator is designed, as shown in Fig. 4(a). It consists of a laser displacement sensor (LDS) (American Electric), a data acquisition device (NI-USB6003, National Instruments, USA), and a computer. The anode is a metal mesh (Zngou Co., China) with 60 mesh, and the thickness is 300 μm [36]; the cathode is a stainless steel sheet with 20 μm thick (Zngou Co., China); the PVC gel is made by mixing PVC powders (the molecular weight is 4400)

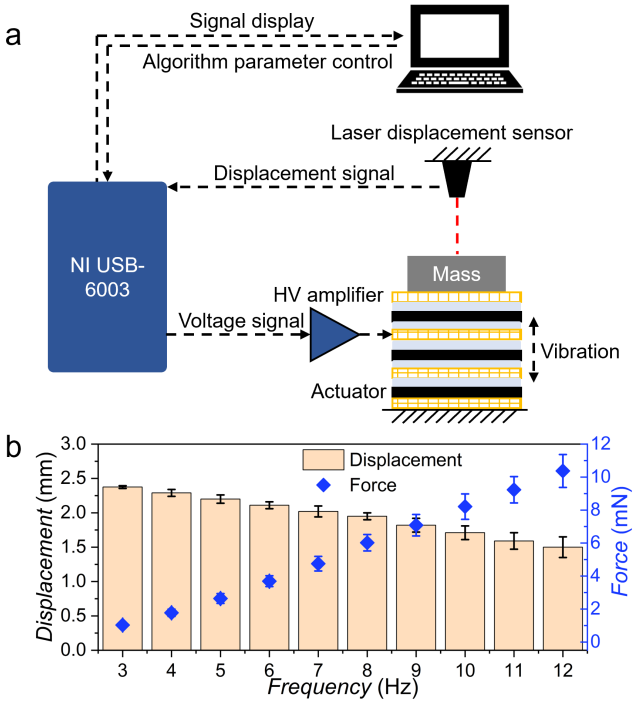

Fig. 4. Tests of actuation performances of the stacked actuator. (a) The testing process: a computer transmits the control signal to the amplifier via NI USB 6003 to generate a voltage signal, then the actuator is triggered to vibrate. The laser displacement sensor above collects the actuator's position change information and sends the data to the computer by NI USB 6003. (b) With different frequencies between 3 and 12 Hz, the stacked actuator produces various displacements and forces.

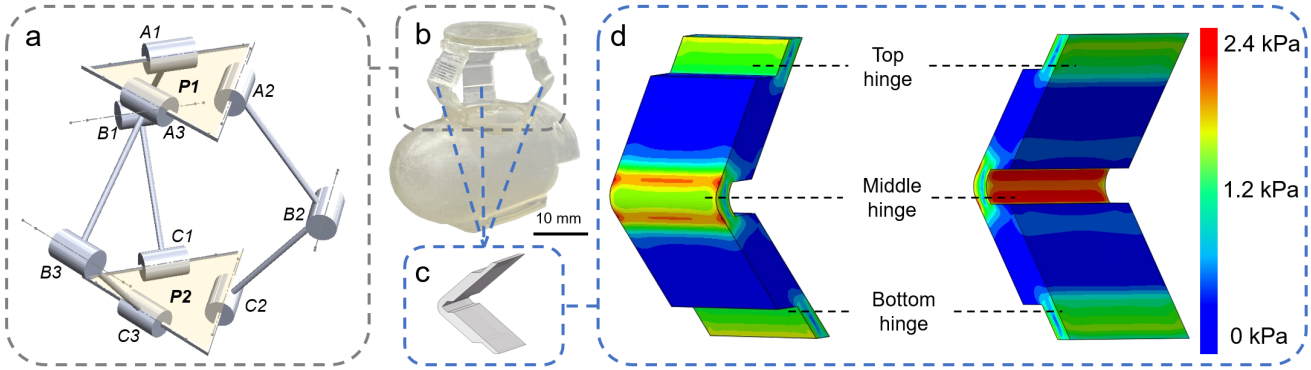

Fig. 5. The Sarrus-mechanism exoskeleton. (a) The principle of the Sarrus mechanism. (b) The image of the exoskeleton. (c) One limb model of the Sarrus mechanism exoskeleton. (d) The FEA of one limb in stretching simulation.

(Scientific Polymer Products, Inc., USA) with dibutyl adipate (DBA) (Sigma-Aldrich, USA) and the ratio is PVC: DBA = 1:4 by weight [36], [42], [43] and a single layer is 400 μm thick. According to the test, the maximum allowed working voltage is 700 V with a current of 100 μA, referencing the previous study [43]. The laser displacement sensor (ILD1402, Micro-Epsilon Co., UK) measures the displacement of the actuator per unit of time and calculates the output vibration force according to Eq. (4), (5), and (6). The data processor NI USB-6003 is applied to collect the data from the LDS and apply the voltage to the stacked actuator via the amplifier.

We apply the maximum voltage of 700 V to the actuator [43] in various frequencies between 3 and 12 Hz, corresponding to the frequency observed in tremors [1]. The results of various displacements and vibration forces (calculated by Eq. (7)) are obtained (Fig. 4(b)). The result shows that the minimum vibration force is 1.03 mN when the frequency is 3 Hz, precisely matching the assumed common finger tremor force of 1 mN. In this configuration, the number of stacked units is determined as 27, and the height and weight of the stacked actuator are measured as 19 mm and 12 g, respectively.

B. Sarrus-mechanism Exoskeleton

Researchers used different housing methods in previous studies on stacked PVC gel actuators. The most typical and commonly used method is using a stick passing through the actuator [32] along the axis of symmetry. This method can help the stacked actuator move linearly without getting loose. However, it sacrifices a certain actuation effect due to the hollow space the stick takes. This is because the actuation area directly impacts the PVC gel actuator's performance: with other conditions being the same, the larger the area, the better the actuating effect [30]. In addition, it causes friction with the central stick when the actuator is actuating, which also makes the actuation less efficient.

Here, we design a 3D printable single-part exoskeleton consisting of a fingertip sleeve and a Sarrus mechanism with flexure hinges as the exoskeleton (Fig. 3(b)) to house the stacked PVC gel actuator without getting loose. The Sarrus mechanism (Fig. 5) consists of two platforms p_1 and p_2, and nine flexure hinges (A_1, B_1, ..., B_3, C_3). The parallel structure of the mechanism allows the actuator to prevent waste in the actuation area and to avoid friction with the stick. In addition, the Sarrus mechanism with straight-line motion can minimize the swaying of the stacked linear actuator. Therefore, the design parameters of the mechanism are the key to guaranteeing its performance [44]. Here, we use segmented thickness 3D printed limbs to realize the function of the hinges, as shown in Fig. 5(c).

Prior to printing, the finite element analysis (FEA) is applied to get an adequate distance between p_1 and p_2, and the hinges' thickness in the software ABAQUS CAE 2020 (ABAQUS Inc., Dassault SIMULIA, USA). This simulation analysis reveals that the middle hinge (Fig. 5(d)) in each limb is the most likely location for breakage. Combined with the actuation force of the stacked actuator (to ensure the stable assembly), the simulation results suggest the minimum thickness for middle hinges (B_1, B_2, B_3) (Fig. 5(a)) and the distance between P_1 and P_2 without load should be 0.42 mm and 17.5 mm, respectively. With these design parameters, the maximum stress happened on the middle hinges when the Sarrus-mechanism skeleton is stretched by the resilience of the PVC gel actuator (the thickness from 17.5 to 19 mm) is around 2 kPa, which is under the break stress (3.1 kPa), as shown in Fig. 5(d). After printing, we tested the cycle life of the hinge: over 518,400 cycles (12 hours) by 12 Hz and 1.6 mm vibration produced by the stacked actuator and over 7,100 cycles (10 min) with ultimate load (3.1 kPa) at 12 Hz and 2.5 mm amplitude produced by Instron E1000 (Instron, U.K.).

C. Control Scheme

The Least Mean Square (LMS) algorithm is a common active vibration control method [45], which is applied for closed-loop control. The LMS algorithm is an adaptive algorithm that uses the gradient-based steepest descent method, as shown in Fig. 6. it adopts an estimate of the gradient vector from the available data [46], which is expressed as

$$w(n+1) = w(n) + \mu \cdot r(n) \cdot e(n) \tag{8}$$

where $w(n)$ and $w(n+1)$ are the weight vectors at point n and $(n+1)$, respectively [47]. $r(n)$ is the input reference signal

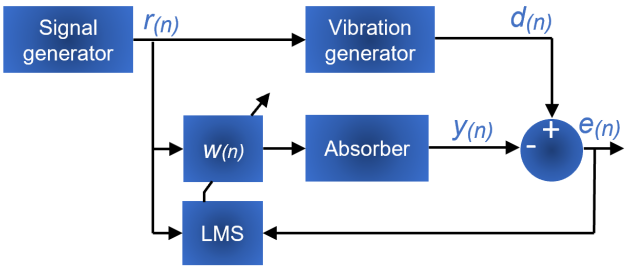

Fig. 6. The closed-loop working process of the LMS algorithm.

vector (the tremor signal) stored in the filter delayed line. μ is the convergence factor of the filter, and it can be obtained by the maximum eigenvalue of the autocorrelation function of the reference signal. $e(n)$ is the error signal (the residual vibration after the suppression detected by the IMU or the force sensor) and can be described by

$$e(n) = d(n) - y(n) \tag{9}$$

where $d(n)$ is the desired signal (the vibration happens on the finger before the suppression that is detected by the IMU or the force sensor). $y(n)$ is the output signal (the vibration produced by the absorber) and is given by

$$y(n) = w(n) \cdot r(n)^T \tag{10}$$

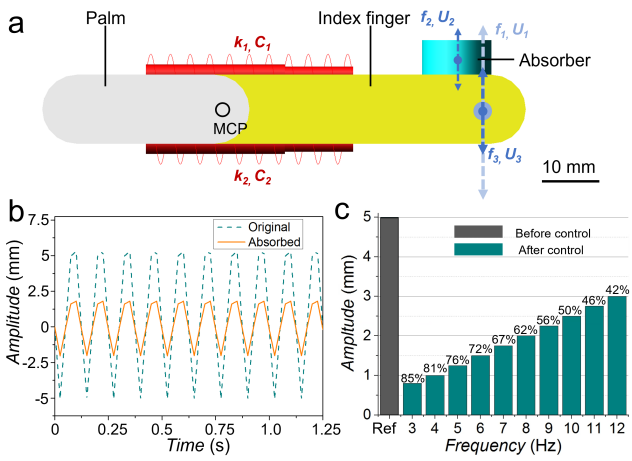

Fig. 7. The vibration dynamic simulation in ADAMS. (a) The analytical model of the vibration motion of a finger. The joint represents the index finger's metacarpophalangeal (MCP) knuckle: with stiffness (k_1=k_2=100 kN/m) and damping (C_1=C_2=0.05). The tremor is f_1U_1; the vibration produced by the absorber is f_2U_2; the residual vibration is f_3U_3. f is the frequency, U is the vibration. The values of f_1, f_2, and f_3 are always the same. (b) The absorbing result in the situation: the tremor amplitude is 5 mm with a frequency of 8 Hz, and the absorber is applied with maximum power (700 V and 100 μA). (c) The suppression results in various tremors (the frequency between 3 and 12 Hz, and the initial amplitude is 5 mm).

IV. Tremor Suppression

A. Vibration Dynamics Simulation

To mimic the finger tremor, we apply a soft rubber tube to represent the index finger (Fig. 8(a) and (b)), whose length is 8 cm (the average length of the index finger of adults) and the weight is 10 grams [48]. The bending stiffness and damping are 100 kN/m and 0.05, respectively, which match the stiffness and damping of the metacarpophalangeal (MCP) joint [49], [50].

To obtain the designed finger-worn active vibration absorber's theoretical working effect, in this section, we present a vibration dynamics simulation model using the dynamics simulation software ADAMS 2017 (MSC Software Corporation, USA), as shown in Fig. 7(a). Two springs with stiffness (k_1=k_2=100 kN/m) and damping (C_1=C_2=0.05) are attached to the MCP joint to connect the index finger and the palm. Firstly, the output amplitude is maintained at 2.5 mm, and then the maximum vibration force is 10 mN (at 12 Hz). The vibration is completely absorbed, and the fingertip amplitude is zero when the absorber is applied with the maximum power (700 V and 100 μA). Then we doubled the amplitude (5 mm, the maximum output vibration force is 24 mN at 12 Hz) to simulate an extreme tremor. For instance, Fig. 7(b) shows the vibration suppression effect when the frequency is 8 Hz, and in this circumstance, the absorber suppresses the vibration to 62%. Fig. 7(c) shows the simulated attenuation effect (the amplitude after the suppression) of different frequencies (between 3 and 12 Hz). When the tremor frequency is 3 Hz, the suppression ratio is 85%. As the frequency increases, the suppression ratio decreases to 42% when the frequency is 12 Hz. That is due to the output power of the tremor increasing (produced by the motor in the vibrator) when the frequency increases as the setting amplitudes are the same (5 mm). However, the maximum absorbing power is fixed (0.7 W) because the maximum voltage and current applied to the PVC gel actuator are 700 V and 100 μA, respectively. Therefore, the suppressed ratio decreases when the frequency increases.

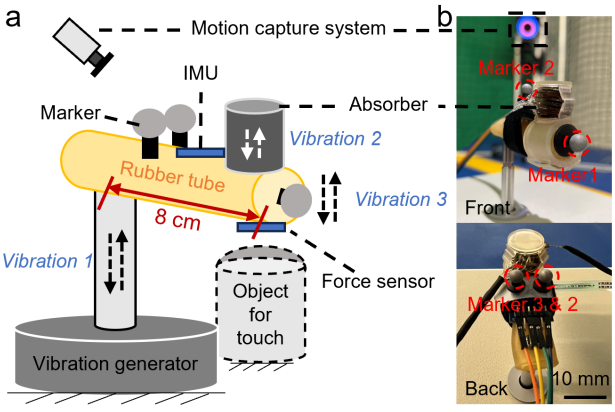

Fig. 8. The testing platform. (a) The schematic of the testing platform. The components include a rubber tube (10 cm long and 1.5 cm in extra diameter), the absorber, the vibration generator, three markers, and the motion capture system. $Vibration1$ is the vibration produced by the vibration generator to mimic the tremor. $Vibration2$ is the vibration produced by the actuator. $Vibration3$ is the vibration that happens on the end of the "finger" before the absorber works. The residual vibration after the suppression can be expressed as ($Vibration3$ - $Vibration2$). (b) Pictures of the platform.

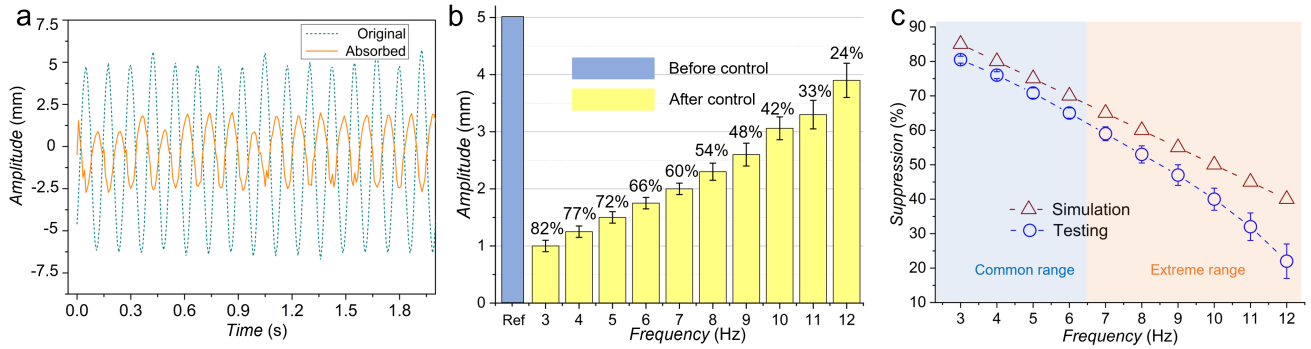

Fig. 9. The testing results. (a) The vibration before and after the absorption at 8 Hz. (b) The vibration amplitude before and after control in various frequencies between 3 and 12 Hz. (c) The comparison between the simulation and tests.

TABLE I
COMPARISON WITH OTHER FINGER TREMOR ABSORBERS

Name of the Device	Actuation Method	Absorbing Type	Response Time (s)	Weight (g)	Tremor Detecting Method
Gyroscopic glove [10]	Gyroscope	Passive	>1	>500	Hand motion
Wearable tremor suppression glove [5]	Motor	Active	1	300	Finger bending
Bending pneumatic artificial muscle [15]	Pneumatic fiber actuator	Active	0.2∼0.3	9.5	Finger bending
Soft exoskeletal glove [16]	Pneumatic actuator	Semi-active	<1	160	Finger bending
This work: AFTO	PVC gel actuator	Active	<0.1	25	Finger bending & force changing

B. Experiments

To verify the absorber's suppression effect, we set a testing platform (Fig. 8(a) and (b)). The absorbing system (the absorber, the exoskeleton, the force sensor, and the IMU) is assembled on one end of the tube. The tube is fixed on the vibration generator (Vibrationsgenerator 1000701, 3B SCIENTIFIC PHYSICS, Germany), which generates vibrations mimicking tremors. The IMU and the force sensor detect tremors by the frequency when the tube is vibrating in the air and touching a temporary item, respectively, as shown in Fig. 8(a). The devices above are placed in a motion capture (MOCAP) space. Three reflective markers are attached to the rubber tube to identify the fingertip as a rigid body, which the MOCAP tracks. The testing devices are connected to Jetson Nano, which is used to decouple the signal from the IMU and the force sensor and is also applied to use the LMS algorithm coded by Python, then send the control signal (voltage) to the stacked actuator via the amplifier.

The testing results are shown in Fig. 9. The amplitude is 5 mm and 2.3 mm before and after the vibration control when the vibration frequency is 8 Hz, as shown in Fig. 9(a). Applying the maximum power (700 V, 100 μA) to the actuator, as shown in Fig. 9(b), the suppression results of various vibrations with frequencies between 3 and 12 Hz are obtained. The residual vibration's amplitude gets bigger when the frequency increases. It is due to the input power of the actuator as a constant value, and when the frequency increases, the actuation force becomes smaller. However, the vibration amplitude provided by the vibration generator is the same (5 mm). When the frequency increases, the output force increases, as shown in Eq. (7). Comparing the results between the simulation and the experiment (Fig. 9(c)), the experimental suppression ratio is slightly lower than the simulation and the difference between the two gets bigger when the frequency increases. The reason is when the actuator vibrates, the damping gets smaller (the higher the frequency, the smaller) in experiments while it keeps constant in the simulation. As is known, sufficient damping helps suppress vibration [51]. This is due to the PVC gel actuator's working principle, namely, the mesh absorbs the gel, which will decrease the damping somehow. This phenomenon can be understood and observed, but the damping change's value is not easy to predict [52]. In addition, the most common frequency of tremors is under 6 Hz [53], [54], as shown in Fig. 9(c). Using the AFTO, the tremor happening on the fingertip can be suppressed over 65%.

C. Comparison with Other Finger Tremor Suppression Devices

To further analyze the performance of the AFTO, we compare it with other finger tremor suppression devices in terms of actuation method, vibration absorbing type, response time, weight, and the method for detecting tremors, as shown in Table I. The AFTO has the unique advantage of being lightweight (25 g) and has a short response time (<0.1 s), which helps eliminate time errors in active vibration reduction. In addition, the AFTO possesses two types of sensors, namely, a force sensor and an IMU. These sensors can detect tremors regardless of whether the finger is flexed or in a static position.

V. CONCLUSIONS

This paper introduces a lightweight (25 g), fast-response (<0.1 s), closed-loop controlled, and active finger orthosis. For the first time, it applies the stacked PVC gel actuator as the active absorber for tremor suppression. The application of the

flexible 3D-printed Sarrus-mechanism exoskeleton addresses the housing of the stacked PVC gel actuator without wasting the actuation area. The combination of an IMU and a force sensor enabled the system to detect tremors, irrespective of whether the fingertip is vibrating without contacting an object or exerting tremor-induced pressure while the fingertip is in contact with a substrate. Both simulations and experiments have confirmed the effective tremor suppression by the active absorption system which is capable of suppressing finger tremors by over 65% when the frequency of tremors is between 3 - 6 Hz, the most common frequency range of finger tremors. The performances demonstrate that the proposed orthosis holds excellent potential for a wide range of applications including enhancing the stability of writing or drawing, preventing inadvertent mouse clicks or holding actions, and improving precision when operating a scalpel or other tools that need fine finger motion.

Future research will explore a multi-material 3D-printed exoskeleton to enhance the stacked actuator's linear guidance and extend the hinges' durability. In addition, we will focus on improving the actuator's output force and refining damping control. This will expand the range of applications and further optimize the attenuation effect for increased efficiency.

REFERENCES

[1] T. Welton, F. Cardoso, J. A. Carr, L.-L. Chan, G. Deuschl, J. Jankovic, and E.-K. Tan, "Essential tremor," *Nature Reviews Disease Primers*, vol. 7, no. 1, p. 83, 2021.

[2] W. Poewe, K. Seppi, C. M. Tanner, G. M. Halliday, P. Brundin, J. Volkmann, A.-E. Schrag, and A. E. Lang, "Parkinson disease," *Nature reviews Disease primers*, vol. 3, no. 1, pp. 1–21, 2017.

[3] M.-K. Pan, Y.-S. Li, S.-B. Wong, C.-L. Ni, Y.-M. Wang, W.-C. Liu, L.-Y. Lu, J.-C. Lee, E. P. Cortes, J.-P. G. Vonsattel *et al.*, "Cerebellar oscillations driven by synaptic pruning deficits of cerebellar climbing fibers contribute to tremor pathophysiology," *Science translational medicine*, vol. 12, no. 526, p. eaay1769, 2020.

[4] H. S. Nguyen and T. P. Luu, "Tremor-suppression orthoses for the upper limb: current developments and future challenges," *Frontiers in Human Neuroscience*, vol. 15, p. 622535, 2021.

[5] Y. Zhou, M. E. Jenkins, M. D. Naish, and A. L. Trejos, "Development of a wearable tremor suppression glove," in *2018 7th IEEE International Conference on Biomedical Robotics and Biomechatronics (Biorob)*. IEEE, 2018, pp. 640–645.

[6] O. Sandoval-Gonzalez, J. Jacinto-Villegas, I. Herrera-Aguilar, O. Portillo-Rodiguez, P. Tripicchio, M. Hernandez-Ramos, A. Flores-Cuautle, and C. Avizzano, "Design and development of a hand exoskeleton robot for active and passive rehabilitation," *International Journal of Advanced Robotic Systems*, vol. 13, no. 2, p. 66, 2016.

[7] G. Wang, H. Wang, W. Gao, X. Yang, and Y. Wang, "Jamming enabled variable stiffness wrist exoskeleton for tremor suppression," *IEEE Robotics and Automation Letters*, 2023.

[8] M. S. Faizan and M. Muzammil, "Hand tremor suppression device for patients suffering from parkinson's disease," *Journal of medical engineering & technology*, vol. 44, no. 4, pp. 190–197, 2020.

[9] S. Gebai, M. Hammoud, and H. Khachfe, "Parametric study of an enhanced passive absorber used for tremor suppression," *Structural Control and Health Monitoring*, vol. 25, no. 7, p. e2177, 2018.

[10] A. S. Wehse, D. Muse, and I. Sun, "Gyroscopic stabilization for uniaxial hand tremors," *Worcester Polytechnic Institute, Tech. Rep*, 2019.

[11] A. Yi, A. Zahedi, Y. Wang, U.-X. Tan, and D. Zhang, "A novel exoskeleton system based on magnetorheological fluid for tremor suppression of wrist joints," in *2019 IEEE 16th International Conference on Rehabilitation Robotics (ICORR)*. IEEE, 2019, pp. 1115–1120.

[12] A. Zahedi, B. Zhang, A. Yi, and D. Zhang, "A soft exoskeleton for tremor suppression equipped with flexible semiactive actuator," *Soft robotics*, vol. 8, no. 4, pp. 432–447, 2021.

[13] P. Tran, S. Jeong, K. R. Herrin, and J. P. Desai, "Hand exoskeleton systems, clinical rehabilitation practices, and future prospects," *IEEE Transactions on Medical Robotics and Bionics*, vol. 3, no. 3, pp. 606–622, 2021.

[14] Y. Wang, X.-J. Liu, and H. Zhao, "Control and implementation of a fluidic elastomer actuator for active suppression of hand tremor," *IEEE Robotics and Automation Letters*, 2023.

[15] J. Wirekoh, N. Parody, C. N. Riviere, and Y.-L. Park, "Design of fiber-reinforced soft bending pneumatic artificial muscles for wearable tremor suppression devices," *Smart Materials and Structures*, vol. 30, no. 1, p. 015013, 2020.

[16] V. Skaramagkas, G. Andrikopoulos, and S. Manesis, "An experimental investigation of essential hand tremor suppression via a soft exoskeletal glove," in *2020 European Control Conference (ECC)*. IEEE, 2020, pp. 889–894.

[17] J. Ahn, J. Gu, J. Choi, C. Han, Y. Jeong, J. Park, S. Cho, Y. S. Oh, J.-H. Jeong, M. Amjadi *et al.*, "A review of recent advances in electrically driven polymer-based flexible actuators: Smart materials, structures, and their applications," *Advanced Materials Technologies*, vol. 7, no. 11, p. 2200041, 2022.

[18] G. D. Goh, G. L. Goh, Z. Lyu, M. Z. Ariffin, W. Y. Yeong, G. Z. Lum, D. Campolo, B. S. Han, and H. Y. A. Wong, "3d printing of robotic soft grippers: Toward smart actuation and sensing," *Advanced Materials Technologies*, vol. 7, no. 11, p. 2101672, 2022.

[19] C. Tang, B. Du, S. Jiang, Q. Shao, X. Dong, X.-J. Liu, and H. Zhao, "A pipeline inspection robot for navigating tubular environments in the sub-centimeter scale," *Science Robotics*, vol. 7, no. 66, p. eabm8597, 2022.

[20] M. Sobczyk, S. Wiesenhütter, J. R. Noennig, and T. Wallmersperger, "Smart materials in architecture for actuator and sensor applications: A review," *Journal of Intelligent Material Systems and Structures*, vol. 33, no. 3, pp. 379–399, 2022.

[21] W. Sun, B. Li, F. Zhang, C. Fang, Y. Lu, X. Gao, C. Cao, G. Chen, C. Zhang, and Z. L. Wang, "Teng-bot: Triboelectric nanogenerator powered soft robot made of uni-directional dielectric elastomer," *Nano Energy*, vol. 85, p. 106012, 2021.

[22] G. Li, X. Chen, F. Zhou, Y. Liang, Y. Xiao, X. Cao, Z. Zhang, M. Zhang, B. Wu, S. Yin *et al.*, "Self-powered soft robot in the mariana trench," *Nature*, vol. 591, no. 7848, pp. 66–71, 2021.

[23] Y. Shi, E. Askounis, R. Plamthottam, T. Libby, Z. Peng, K. Youssef, J. Pu, R. Pelrine, and Q. Pei, "A processable, high-performance dielectric elastomer and multilayering process," *Science*, vol. 377, no. 6602, pp. 228–232, 2022.

[24] P. Rothemund, N. Kellaris, S. K. Mitchell, E. Acome, and C. Keplinger, "Hasel artificial muscles for a new generation of lifelike robots—recent progress and future opportunities," *Advanced Materials*, vol. 33, no. 19, p. 2003375, 2021.

[25] Y. Qiu, E. Zhang, R. Plamthottam, and Q. Pei, "Dielectric elastomer artificial muscle: materials innovations and device explorations," *Accounts of chemical research*, vol. 52, no. 2, pp. 316–325, 2019.

[26] J. Wang, D. Gao, and P. S. Lee, "Recent progress in artificial muscles for interactive soft robotics," *Advanced Materials*, vol. 33, no. 19, p. 2003088, 2021.

[27] C. Wang, R. Li, Z. Zhu, J. H. Wu, and F. Ma, "A pvc plasticization electrically active laminated metamaterial with tunable sound insulating performance," *Engineering Structures*, vol. 269, p. 114777, 2022.

[28] M. Ali, T. Ueki, D. Tsurumi, and T. Hirai, "Influence of plasticizer content on the transition of electromechanical behavior of pvc gel actuator," *Langmuir*, vol. 27, no. 12, pp. 7902–7908, 2011.

[29] Z. Frank, M. Al-Rubaiai, X. Tan, and K. J. Kim, "A study of electroactive polyvinyl chloride (pvc) gel actuators through the use of the electric modulus formalism and cyclic linear voltage sweeps," *Smart Materials and Structures*, vol. 31, no. 3, p. 035020, 2022.

[30] C. Dong, Z. Zhu, Z. Li, X. Shi, S. Cheng, and P. Fan, "Design of fishtail structure based on oscillating mechanisms using pvc gel actuators," *Sensors and Actuators A: Physical*, vol. 341, p. 113588, 2022.

[31] N. Ogawa, M. Hashimoto, M. Takasaki, and T. Hirai, "Characteristics evaluation of pvc gel actuators," in *2009 IEEE/RSJ International Conference on Intelligent Robots and Systems*. IEEE, 2009, pp. 2898–2903.

[32] Y. Li and M. Hashimoto, "Pvc gel based artificial muscles: Characterizations and actuation modular constructions," *Sensors and Actuators A: Physical*, vol. 233, pp. 246–258, 2015.

[33] R. Liu, Y.-a. Yao, and Y. Li, "Design and analysis of a deployable tetrahedron-based mobile robot constructed by sarrus linkages," *Mechanism and Machine Theory*, vol. 152, p. 103964, 2020.

[34] B. Widrow, J. McCool, and M. Ball, "The complex lms algorithm," *Proceedings of the IEEE*, vol. 63, no. 4, pp. 719–720, 1975.

[35] D. J. Inman, *Vibration with control*. John Wiley & Sons, 2017.
[36] Y. Li, Y. Li, and M. Hashimoto, "Low-voltage planar pvc gel actuator with high performances," *Sensors and Actuators B: Chemical*, vol. 282, pp. 482–489, 2019.
[37] M. Hashimoto, "Development of an artificial muscle using pvc gel," in *ASME International Mechanical Engineering Congress and Exposition*, vol. 54884, 2011, pp. 745–754.
[38] S. Komandur, P. W. Johnson, R. L. Storch, and M. G. Yost, "Relation between index finger width and hand width anthropometric measures," in *2009 Annual International Conference of the IEEE Engineering in Medicine and Biology Society*. IEEE, 2009, pp. 823–826.
[39] F. Budini, L. Labanca, M. Scholz, and A. Macaluso, "Tremor, finger and hand dexterity and force steadiness, do not change after mental fatigue in healthy humans," *Plos one*, vol. 17, no. 8, p. e0272033, 2022.
[40] D. E. Vaillancourt, A. B. Slifkin, and K. M. Newell, "Regularity of force tremor in parkinson's disease," *Clinical Neurophysiology*, vol. 112, no. 9, pp. 1594–1603, 2001.
[41] M. N. Alam, B. Johnson, J. Gendreau, K. Tavakolian, C. Combs, and R. Fazel-Rezai, "Tremor quantification of parkinson's disease-a pilot study," in *2016 IEEE International Conference on Electro Information Technology (EIT)*. IEEE, 2016, pp. 0755–0759.
[42] Z. Frank and K. J. Kim, "On the mechanism of performance improvement of electroactive polyvinyl chloride (pvc) gel actuators via conductive fillers," *Scientific Reports*, vol. 12, no. 1, p. 10316, 2022.
[43] C. Liu, J. J. Busfield, and K. Zhang, "An electric self-sensing and variable-stiffness artificial muscle," *Advanced Intelligent Systems*, p. 2300131, 2023.
[44] F. Guo, T. Sun, P. Wang, S. Liu, B. Lian, and Y. Song, "Multi-stability of a planar three-limb flexible mechanism," *Mechanism and Machine Theory*, vol. 175, p. 104956, 2022.
[45] Z. Li, M. Sheng, M. Wang, P. Dong, B. Li, and H. Chen, "Stacked dielectric elastomer actuator (sdea): casting process, modeling and active vibration isolation," *Smart Materials and Structures*, vol. 27, no. 7, p. 075023, 2018.
[46] C. Zhou, H. Zou, and X. Qiu, "A frequency band constrained filtered–x least mean square algorithm for feedback active control systems," *The Journal of the Acoustical Society of America*, vol. 148, no. 4, pp. 1947–1951, 2020.
[47] R. S. A. Araújo, J. C. Tironi, W. D. Parreira, R. C. Borges, J. F. De Paz Santana, and V. R. Q. Leithardt, "Analysis of adaptive algorithms based on least mean square applied to hand tremor suppression control," *Applied Sciences*, vol. 13, no. 5, p. 3199, 2023.
[48] M. Peters, K. Mackenzie, and P. Bryden, "Finger length and distal finger extent patterns in humans," *American Journal of Physical Anthropology: The Official Publication of the American Association of Physical Anthropologists*, vol. 117, no. 3, pp. 209–217, 2002.
[49] N. Sharma and M. Venkadesan, "Finger stability in precision grips," *Proceedings of the National Academy of Sciences*, vol. 119, no. 12, p. e2122903119, 2022.
[50] J. Park, N. Pažin, J. Friedman, V. M. Zatsiorsky, and M. L. Latash, "Mechanical properties of the human hand digits: Age-related differences," *Clinical Biomechanics*, vol. 29, no. 2, pp. 129–137, 2014.
[51] S. H. Crandall, "The role of damping in vibration theory," *Journal of sound and vibration*, vol. 11, no. 1, pp. 3–IN1, 1970.
[52] A. D. Nashif, D. I. Jones, and J. P. Henderson, *Vibration damping*. John Wiley & Sons, 1991.
[53] M. F. Dirkx and M. Bologna, "The pathophysiology of parkinson's disease tremor," *Journal of the Neurological Sciences*, p. 120196, 2022.
[54] A. Channa, R.-C. Ifrim, D. Popescu, and N. Popescu, "A-wear bracelet for detection of hand tremor and bradykinesia in parkinson's patients," *Sensors*, vol. 21, no. 3, p. 981, 2021.